LOCATING TARGETS FOR CRISM BASED ON SURFACE MORPHOLOGY AND INTERPRETATION OF THEMIS DATA. K. Nogeire and M. S. Robinson, Northwestern University 1850 Campus Drive Evanston, IL, 60208

Introduction: The Compact Reconnaissance Imaging Spectrometer for Mars (CRISM) is one of several instruments on the Mars Reconnaissance Orbiter (MRO) to be launched in August 2005. Data from the CRISM spectrometer will be used to globally map the geology, composition and stratigraphy of Mars at a scale of 200 m/pixel. CRISM's overarching objective is to search for evidence of aqueous and hydrothermal deposits. CRISM is also able to acquire high resolution local area spectra at ~20 m/pixel. A list of targets of high science value is being complied based on all available data. Unraveling local geology requires spectral measurements of local rocks. Therefore, CRISM has the greatest possibility of sending back information describing local geology by targeting locations with exposed rock (bedrock or boulders close to their source). The most imposing obstacle to accomplishing this objective is the ubiquitous fine-grained dust that covers nearly all of the surface. The goal of this work is to identify exposed rock in many diverse regions on the martian surface.

Potential rock targets are identified through terrain analysis and interpretation of Thermal Emission Imaging System (THEMIS) thermal imaging data. Morphologic analysis of terrain can help lead an analyst to exposed rock. For example, bedrock in large basins and smaller synclines is likely to be buried in dust. An exposed ledge on a windy canyon wall, on the other hand, could possibly exhibit dust-free, exposed rock. If the thermal signature of this ledge also indicates a cohesive unit, it is likely this ledge will provide a spectral signature that is unique to the rock found in that particular region.

THEMIS thermal imaging represents the best available indicator of blocky terrain, be it boulders or in-situ bedrock. Targets identified in this work are typically dominated by materials with high nighttime temperatures and low albedo, which most likely represent materials with high thermal inertia. Materials with high thermal inertia stay warm long after the sun goes down and thus are easily identified in a nighttime thermal image. As a general rule for Mars, high albedo areas are covered with very fine-grained dust and thus have low thermal inertia, whereas low albedo areas are composed of larger particles which have high thermal inertia [2, 3, 5, 7]. This rule may be violated in the case where fine grain, high albedo material has been indurated thus increasing its thermal inertia. Of course any materials of unusual composition also might violate this rule.

Method: THEMIS consists of two imaging subsystems: a 5 band visible imager (.425 to .860 μm) with a resolution of 19 m/pixel and a 10 band thermal infrared imager (6 to 15 μm) at 100 m/pixel. The high resolution visible images are used to compare relative albedos and analyze terrain. The shortest wavelength bands in the daytime (6.78 μm) and nighttime (8.56 μm) are utilized because atmospheric absorption by dust, H_2O, and CO_2 causes increased interference in wavelengths longer than about 8 microns.

Accompanying each target or set of targets is a discussion which includes a background of known local geology and a description and interpretation of the THEMIS data. The normalized albedo ratio (AR) is the ratio of the target's albedo to the average albedo of the region. The daytime brightness ratio (DBR) and nighttime brightness ratio (NBR) are normalized in the same way as the albedo ratio. A low DBR and high NBR is due to a target which is relatively cool during the day and warm at night, indicating a relatively high thermal inertia.

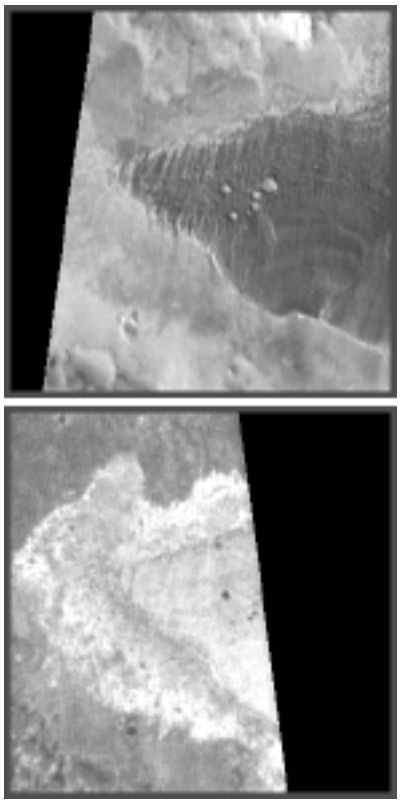

Fig. 1. Arrowhead formation at Bequerel Crater (top=daytime, bottom= nightime THEMIS).

	Target name	Latitude	Longitude	Age [4, 13]	Target type	AR	DBR	NBR
1	Bequerel Crater	21.4 N	351.8 E	Early Hesperian	Mesa	1.5	1	2.2
2	Henry Crater	10.4 N	24.0 E	Mid-Noachian	Crater infill	.84	1.46	6
3	Gusev Crater	14.8 S	175.6 E	Late Hesperian	Crater floor	.82	1.15	2.57
4	Terra Sabaea Crater	1.0 N	26.7 E	Mid-Noachian	Crater infill	-	.89	7.5
5	Kasei Vallis	23.1 N	296.2 E	Late Hesperian	Valley floor	-	2	2.55
6	Mamers Vallis	43.2 N	10.36 E	Late Hesperian	Valley floor	.85	.78	2.26
7	U. Ares Vallis	.84 N	341.5 E	Late Hesperian	Canyon floor	-	.98	1.5
8	U. Ares Vallis	3.0N	342.08 E	Late Hesperian	Canyon ledge	-	.8	2.2

(This is a sample of the target archive. Each target is complimented by a section of the image archive, which holds information on all the images used to view the target)

Target 1: Bequerel crater is partially buried and found in western Arabia Terra, a region dominated by ridged plains material (Hr) formed in the early Hesperian [4]. The target feature in Bequeral is an arrowhead-shaped mesa on the crater floor with unusual thermal properties. The AR for the mesa top is 1.5, the DBR is 1, and the NBR is 2.2. The talus surrounding the mesa has a lower albedo than the mesa top (AR of 1.1). The NBR, on the other hand is equal to that of the mesa top. The talus would likely have a high thermal inertia due to its high population of large debris pieces. The mesa top may be composed of duricrust; in which fine-grained, high albedo dust was cemented together. This would explain the high albedo and apparent high thermal inertia of the mesa top. The visible images show streaks across the top of the mesa which are most likely due to wind. A windy environment explains the dust free surface and rapid erosion of the mesa.

Target 2: Henry crater is partially sediment filled and is located on the border of the high-elevation, heavily-cratered Terra Sabaea and the lower-elevation Arabia Terra. The geologic unit (Npld) prevalent in this region is defined as a heavily cratered unit from the middle Noachian [13], with a higher concentration of channels and increased erosion likely due to fluvial processes [13]. A large hill of sediments has formed within Henry crater with a low albedo, high apparent thermal inertia unit on its east flank. The AR is 0.84, the DBR is 1.46 and the NBR is 6. This target's relatively high DBR and high NBR combined with its low AR make it anomalous amongst most martian material examined in this study.

Target 3: Gusev crater lies on the northern border of the middle Noachian-aged highland unit (Npl_1) and is partially filled with late Hesperian aged channel material (Hch) [13]. An anomalous unit exists on the crater floor with an AR of .82, a DBR of 1.15 and a NBR of 2.57. Although the NBR indicates a lower relative thermal inertia than the relatively high values seen in the Terra Sabaea crater (Table 1), this target remains interesting due to the proposal that the material infilling Gusev crater was formed in an aqueous environment. Most likely this material was exposed by eolian scouring and may represent the underlying geology.

Target 8: Upper Ares Vallis is the source of a major outflow channel. This region is composed of the geologic units (Hch) and (Hcht) [13]. These units are older channel, flood plain and chaotic material from the late Hesperian [13]. The chaotic material at the head of the outflow channels typically exhibit some highland materials [13]. In the case of this target the highland materials would be (Npl_1), a cratered geologic unit from the middle Noachian. With a DBR of .8 and a NBR of 2.2 this target in upper Ares Vallis doesn't appear to have a thermal inertia as high as some of the crater infills.. This thermal signature exists only on this one shelf and is consistent along the entire shelf, possibly indicating unique conditions.

References

[1] Bandfield J. (2002) JGR 107, E6, 10.1029/2001JE001510. [2] Christensen P. (1986) JGR 91, 3533-3545. [3] Golombek M. P. (2003) JGR 108(E12), 8072. [4] Greeley R. and Guest J. (1987) USGS Western region map, 1:15million. [5] Jakosky B. (1986) Icarus 66, 117-124. [6] Jakosky B. and Mellon M. et al. (2000) JGR 105, E4, pp. 9643-9652. [7] Kieffer et al. (1977) JGR 82, 4249-4291. [8] Mellon M. and Jakosky B. et al. (2000) Icarus, 148, 437-455. [9] Pleskot L. and Miner E. (1981) LPI Contribution, no. 441, pp. 208-210. [10] Rees W. (1990) Cambridge University Press. [11] Ruff S. and Christensen P. (1999) LPI Contribution, Report: 972, abstract 6230. [12] Ruff S. and Christensen P. (2002) JGR 107, E12, 5127, 10.1029/2001JE001580. [13] Scott D. and Tanaka K. (1986) USGS Eastern region map, 1:15million.